ROYAL SOCIETY OF CHEMISTRY

PAPER

Check for updates

Degradation pathways of penthiopyrad by δ-MnO₂ mediated processes: a combined density functional theory and experimental study†

Ruishuang Xu, [ab] Mengjiu Zhao, [a] Zhengqiang Chen, [a] Zhihong Gao, [c] Haiyan Song, [iD] *[a] Taicheng An, [iD] [d] Shengrun Zheng [iD] [a] and Fenglong Gu [iD] *[ab]

Penthiopyrad is a widely used succinate dehydrogenase inhibitor (SDHI) fungicide and frequently detected in natural environments. In order to better understand its fate in natural systems, the degradation of penthiopyrad by manganese dioxide (MnO₂) was investigated in this study. The results show that penthiopyrad is rapidly degraded in the δ-MnO₂ system. Moreover, density functional theory (DFT) calculations reveal that the atoms of C18, C12, and S1 in penthiopyrad have relatively high reactive active sites. The degradation products mainly include sulfoxides, sulfones, and diketone. A sulfoxide and sulfone are formed by the oxidation of the thioether group, and diketone is formed by the oxidation of the olefin group, respectively. Based on the DFT calculations and degradation products, the degradation pathway of penthiopyrad by MnO₂ is proposed. This study also reveals that the degradation of penthiopyrad by δ-MnO₂ is affected by various environmental factors. A warm environment, low pH, and co-existing humic acid are beneficial to the degradation of penthiopyrad in the δ-MnO₂ system, whereas, co-existing metal cations inhibit penthiopyrad degradation. This result provides theoretical guidance for predicting the potential fate of penthiopyrad in natural environments.

Environmental significance

The residues of penthiopyrad have negative impacts on the ecosystem. The oxidative degradation of penthiopyrad in the δ-MnO₂ system is investigated in this study. The degradation products of sulfoxide and sulfone were formed by the oxidation of thioether in penthiopyrad, and the product of diketone was formed by the oxidation of olefin in penthiopyrad. The degradation pathway of penthiopyrad in the MnO₂ system is proposed based on products and density functional theory. These results are very useful for ecological risk assessment and remediation of penthiopyrad contaminating the environment.

1. Introduction

Succinate dehydrogenase inhibitor (complex II or succinate–ubiquinone oxidoreductase, SDHI) fungicides play an important role in the comprehensive management of various plant fungal diseases, such as rust and diseases caused by Basidiomycets and *Rhizoctonia*.[1,2] They can block ubiquinone binding sites in the mitochondrial complex II to specifically inhibit

[a]*School of Chemistry, South China Normal University, Guangzhou 510006, PR China. E-mail: songhaiyan@m.scnu.edu.cn; gu@scnu.edu.cn; Tel: +86-20-39310253; +86-20-39310187*

[b]*Key Laboratory of Theoretical Chemistry of Environment, Ministry of Education, School of Chemistry, South China Normal University, Guangzhou 510006, PR China*

[c]*Analysis and Testing Center, South China Normal University, Guangzhou 510006, PR China*

[d]*Guangzhou Key Laboratory of Environmental Catalysis and Pollution Control, School of Environmental Science and Engineering, Institute of Environmental Health and Pollution Control, Guangdong University of Technology, Guangzhou 510006, PR China*

† Electronic supplementary information (ESI) available. See DOI: 10.1039/d1em00339a

fungal respiration, thus leading to fungi death and achieving a bactericidal purpose. In the last ten years, SDHI fungicides (*e.g.* penthiopyrad, flutolanil, boscalid, thifluzamid, and fluxapyroxad) have been one of the fastest growing classes of fungicides in agriculture in many countries, due to their high efficiency and rapid penetration.[3,4] These SDHI fungicides are detected frequently in harvested products, soil, and wastewater.[5–9] As organic contaminants with toxicity, SDHI fungicides have adverse impacts on ecosystems and human health;[10,11] for instance, SDHI causes many human diseases including cancers and neurodegenerative disorders.[10,12]

Penthiopyrad [IUPAC name: (*RS*)-*N*-[2-(1,3-dimethylbutyl)-3-thienyl]-1-methyl-3-(tri-fluoromethyl)pyrazole-4-carboxamide] is one of the most popular SDHI fungicides with a broad spectrum of fungicidal activity. Penthiopyrad has been introduced into the environment by intensive spraying on various vegetables and fruits.[13,14] Under field conditions, 90 percent dissipation (DT₉₀) of penthiopyrad requires 169 days or more than 1000 days in the laboratory.[15] The biodegradation efficiencies of penthiopyrad are only 5% and 34.2% upon treatment with *B.*

subtilis and *T. harzianum* strains during 14 days of incubation, respectively.[16] Moreover, penthiopyrad is also relatively stable to photodegradation because it is specially designed for usage in farmland. Therefore, the residues of penthiopyrad accumulated in fruits or vegetables and natural environments and have negative impacts on ecosystems and human health.[6,8,17–19]

Studies have demonstrated that abiotic degradation of organic contaminants by metal oxides (*e.g.*, MnO_2, FeOOH and Fe_2O_3) is an important reaction in natural environments.[20,21] MnO_2 is the most important naturally occurring reactant or catalyst in soil and sediments, and plays a significant role in the abiotic processes of organic pollutants in natural systems.[22,23] Due to a high standard redox potential of 1.23 V, MnO_2 can degrade many organic contaminants, including phenols.[23–26] Penthiopyrad is a kind of imidazole pesticide; therefore it is possible to be degraded by MnO_2 based on theory; however, knowledge on this degradation processes is still limited and further investigation is warranted.

The objectives of this work are to investigate the degradation pathways of penthiopyrad mediated by δ-MnO_2. For this purpose, (1) the degradation kinetics of penthiopyrad in the δ-MnO_2 system was discussed; (2) the degradation products of penthiopyrad were identified; (3) the reactive active sites of penthiopyrad were determined by density functional theory (DFT) calculations and (4) the degradation pathways of penthiopyrad were elucidated. In addition, the influences of environmental factors, such as pH, metal ions, and humic acid (HA) were also discussed in this study. These results are important for predicting the environmental behavior of penthiopyrad and evaluating its potential risks in natural environments.

2. Materials and methods

2.1. Chemicals and stock preparation

Penthiopyrad (>98%, Shanghai Yuanye Bio-Technology Co., Shanghai, China), humic acid (AR, Shanghai Macklin Biochemical Co., Ltd., Shanghai, China), MeOH (HPLC, Tedia, Fairfield, OH, USA), and other reagents (AR, Guangzhou Chemicals Inc. Guangzhou, China) were used in this study. A Waters Oasis HLB column (500 mg/6 mL) was purchased from Waters Corporation (Massachusetts USA). A stock solution of penthiopyrad (50 μmol L^{-1}) was prepared and stored at 4 °C without light, and was diluted to the desired concentration during the experiment. Solutions of inorganic ions (Mn^{2+}, Ca^{2+}, and Mg^{2+}) were obtained by dissolving the corresponding chloride salt in buffer solution and the concentrations of ions were adjusted to 0.1 mmol L^{-1}.

2.2. Methods

2.2.1 δ-MnO_2 preparation and characterization. δ-MnO_2 was synthesized following the method in a previous study.[27] 40 mL of 0.014 mol L^{-1} $MnSO_4 \cdot H_2O$ was added dropwise into 40 mL of 0.1 mol L^{-1} $KMnO_4$ solution under constant stirring. Then the mixed solution was continuously stirred for one hour. After that, the mixture was transferred and sealed in a Teflon-lined autoclave and kept at 160 °C for 4 h. The product was

then cooled to room temperature and washed with Milli-Q water several times until no SO_4^{2-} was detected in the washing solution by Ba^{2+} testing. The product was dried in air at 60 °C overnight.

The phase identification of synthesized δ-MnO_2 was characterized by powder X-ray diffraction (XRD, UltimalV, Shimadzu, Japan) (Fig. S1†). The characteristic stretching vibration peak of the δ-MnO_2 unit cell was identified using a Fourier-transform infrared spectrometer (FTIR, Spectrum Two, PerkinElmer, German) (Fig. S2†). The specific surface area of δ-MnO_2 is measured to be 40.92 m^2 g^{-1} using an ASAP-2460 Analyzer (Micromeritics, The U.S.A.) (Fig. S3†). The different oxidation state Mn contents are presented in Fig. S4† as observed by XPS (K-Alpha+, Thermo Fisher Scientific, The U.S.A.). A small amount of Mn^{2+} exists on the surface of δ-MnO_2. The morphology of the δ-MnO_2 is a flower shape obtained using a scanning electron microscope (SEM ZEISS Gemini 500, Carl Zeiss, German) (Fig. S5†).

2.2.2 Penthiopyrad degradation. Degradation of penthiopyrad by δ-MnO_2 was conducted in 15 mL amber bottles with Teflon caps. These amber bottles were kept under stirring in a shaker to maintain a semi-homogenous solution. The reaction solutions were maintained at a constant pH with 10 mmol L^{-1} of acetic acid (HAc)–sodium acetate (NaAc) buffer and a constant ionic strength with 10 mmol L^{-1} NaCl. Certain amounts of reaction solutions were collected at periodic time intervals and quenched immediately by rapid filtration through 0.22 μm nylon 66 membranes (Millipore). Besides, in order to explore the adsorption of manganese dioxide to penthiopyrad, L-ascorbic acid was used to quench the reaction by dissolving the residual δ-MnO_2 solid. Then the filtrates were immediately analyzed by the HPLC method. At the same time, a blank experiment without manganese dioxide was performed to evaluate the stability of penthiopyrad. All experiments were performed in triplicate.

In order to obtain adequate reaction intermediates and possible degradation products, the reaction was quenched after 10.5 h by adding oxalic acid. Then all the solution samples were concentrated and extracted with the HLB column. Then the products of penthiopyrad were analyzed by HPLC-Q-TOF-MS.

2.2.3 Analytical methods. Penthiopyrad concentrations were determined by high-performance liquid chromatography (HPLC, Agilent 1260II, Agilent, the U.S.A, XDB-C18, 4.6 × 150 mm, 5 μm) at 228 nm with the injection volume of 50 μL. The mobile phase was 25% Milli-Q water containing 0.1% phosphoric acid aqueous solution and 75% acetonitrile at a flow-rate of 0.6 mL min^{-1}.

The degradation products of penthiopyrad were analyzed using an Agilent 1290II-6545 HPLC-Q-TOF-MS with an electron-ionization (ESI) interface. To measure the mass spectra of target compounds and their substructures, TOF-MS/MS was performed in full-scan mode. The mobile phase contained 0.1% acetic acid (v/v) in Milli-Q water and acetonitrile in positive and negative electrospray ionization modes. By comparing the chromatographic retention time and ESI-MS spectral data, the products were identified.

2.2.4 Theoretical calculations. Theoretical calculations based on density functional theory (DFT) were performed using Gaussian 09 and Multiwfn software.[28,29] Geometry was optimized at the M06-2X/6-31G* level for penthiopyrad. And the solvent effects were determined by using the SMD model.[30] The Fukui function was also used to evaluate the radical (f^0), nucleophilic (f^+) and electrophilic (f^-) sites.[31,32] More details on DFT calculations can be found in the ESI.†

3. Results and discussion

3.1. Reaction kinetics of penthiopyrad degradation by δ-MnO₂

Fig. 1 shows a typical degradation profile of penthiopyrad at 10 mmol L⁻¹ NaCl as a background electrolyte at pH 4.0. It can be observed that the penthiopyrad concentration is rapidly decreased in the δ-MnO₂ system and the degradation efficiencies of penthiopyrad are enhanced when the δ-MnO₂ concentration increased from 50 mg L⁻¹ and 200 mg L⁻¹ (Fig. 1a and b). In the control experiment, penthiopyrad is stable, no degradation is observed within 630 min without δ-MnO₂, and δ-MnO₂ is also stable and no Mn²⁺ is detected in the absence of penthiopyrad. Moreover, to study the effect of δ-MnO₂ adsorption on the degradation process of penthiopyrad, except for the filtration method to quench the reaction, L-ascorbic acid is also added into the reaction solution to dissolve the residual δ-MnO₂.[33] As shown in Fig. 1a, the residual penthiopyrad concentration by L-ascorbic acid quenching is slightly lower than that by filtration quenching for the first 180 min. However, the final residual penthiopyrad concentrations by L-ascorbic acid quenching and filtration quenching are approximately equal, which is similar to that observed in degradation of chlortetracycline by manganese dioxide and suggests that the adsorption of penthiopyrad on δ-MnO₂ is negligible.[34] Therefore, our results certainly indicate that penthiopyrad can be rapidly degraded in the δ-MnO₂ system.

In general, the degradation of organic contaminants in the manganese oxide system includes two main steps: the formation of precursor complexes between the organic contaminant

and manganese oxide, and electron transfer within the precursor complexes.[35] However it is difficult to distinguish the effect of a single factor on the degradation of organic pollutants without detailed knowledge about the relevant fundamental reaction. Currently, mechanism-based models have been proved to be a perfect method to predict the kinetics of the organic compound degradation.[35–38] Among these models, the complex model has been successfully used to fit the degradation kinetics of some organic contaminants with varying structural characteristics.[35,38,39] In this study, the degradation kinetics of penthiopyrad in the δ-MnO₂ system is also fitted by the complex model. In the complex model, the formation of precursor complexes or the transfer of electrons may be the rate-limiting step. If the formation of precursor complexes is the rate-limiting step, the degradation kinetics of penthiopyrad can be fitted by eqn (1), which is a pseudo-second-order equation.

$$C = \frac{S_1 - C_0}{\dfrac{S_1}{C_0}e^{k_1(S_1 - C_0)t} - 1} \tag{1}$$

Contrarily, if the transfer of electrons is the rate-limiting step, the degradation kinetics of penthiopyrad can be fitted by eqn (2), which is a pseudo-first-order equation.

$$C = (C_0 - S_2) + S_2 e^{-k_2 t} \tag{2}$$

where C_0 (in μM) and C (in μM) are the concentrations of penthiopyrad at time zero and time t (in min), respectively, k_1 (in μM⁻¹ min⁻¹) and k_2 (in min⁻¹) are the reaction apparent rate constants, and S_1 (in μM) and S_2 (in μM) represent the total reactive surface sites that degraded the penthiopyrad.

According to eqn (1) and (2), the total reactive surface sites and the apparent rate constant are evaluated by fitting experimental data, and the fitting degrees of experimental data are all perfect ($R^2 > 0.95$) (Table 1). However, reaction kinetics can be fit by a certain model, which does not necessarily mean that both reaction mechanism models were applicable in the simulation system. As shown in Table 1, the rate constants (k_1 and k_2) are obviously affected by the δ-MnO₂ concentration and
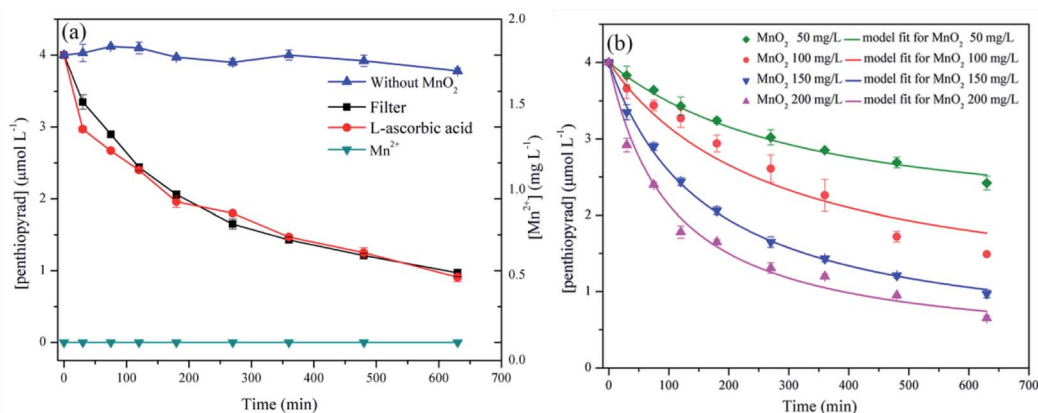
Fig. 1 The degradation profile of penthiopyrad in the δ-MnO₂ system [NaCl]₀ = 10 mmol L⁻¹, pH = 4. (a) The time courses of penthiopyrad and generation of Mn²⁺; (b) effect of the concentration of MnO₂ on penthiopyrad degradation [penthiopyrad]₀ = 4 μmol L⁻¹.

Table 1 The apparent rate constants of penthiopyrad degradation in the δ-MnO$_2$ system were simulated using eqn (1) and (2)

T (°C)	pH	δ-MnO$_2$ (mg L^{-1})	Penthiopyrad (µM)	Eqn (1)			Eqn (2)		
				S_1 (µM)	$k_1 \times 10^{-3}$ (µM^{-1} min^{-1})	R_1^2	S_2 (µM)	$k_2 \times 10^{-3}$ (min^{-1})	R_2^2
30	4.00	50	4.00	1.80	0.88 ± 0.03	0.993	1.82	2.90 ± 0.07	0.996
30	4.00	100	4.00	2.83	0.95 ± 0.09	0.955	2.70	3.08 ± 0.18	0.979
30	4.00	150	4.00	3.56	1.59 ± 0.03	0.998	2.99	6.14 ± 0.22	0.994
30	4.00	200	4.00	3.65	2.58 ± 0.15	0.986	3.20	8.72 ± 0.80	0.964
30	4.00	150	2.12	1.95	2.99 ± 0.15	0.990	1.75	4.95 ± 0.16	0.994
30	4.00	150	4.00	3.56	1.59 ± 0.03	0.998	2.99	6.14 ± 0.22	0.994
30	4.00	150	7.15	5.86	1.47 ± 0.15	0.952	5.00	12.17 ± 0.69	0.992

penthiopyrad concentration in this reaction system. This result indicates that the formation of precursor complexes is the rate-limiting step in the degradation of penthiopyrad by δ-MnO$_2$.[35] Therefore, the degradation kinetics of penthiopyrad by δ-MnO$_2$ is analysed using eqn (1) in the present study.

It is obvious that the total reactive surface sites (S_1) and the apparent rate constant (k_1) are increased with the increasing δ-MnO$_2$ concentrations, when the concentration of penthiopyrad remains constant. As shown in Table 1, the S_1 values and the k_1 values increase from 1.80 µM to 3.65 µM and from 0.88 × 10^{-3} µM^{-1} min^{-1} to 2.58 × 10^{-3} µM^{-1} min^{-1}, respectively, with the increasing initial δ-MnO$_2$ concentrations from 50 mg L^{-1} to 200 mg L^{-1}. The increases of the S_1 values and the k_1 values are attributed to the increase in the number of total reaction active sites on the surface of δ-MnO$_2$ with increasing initial δ-MnO$_2$ concentrations. However, the changes of S_1 values and k_1 values with the δ-MnO$_2$ concentration are not linear (Fig. S6†), suggesting that the degradation of penthiopyrad in the δ-MnO$_2$ system is a very complex physical and chemical process.

On the other hand, the S_1 values increase but the k_1 values decrease with the increasing initial penthiopyrad concentrations, when the concentration of δ-MnO$_2$ remains constant. As shown in Table 1, the S_1 values increase from 1.95 µM to 5.68 µM with the increasing initial penthiopyrad concentrations from 2.12 µM to 7.15 µM, which can be explained by the fact that a high concentration of penthiopyrad occupies more surface reactive sites of MnO$_2$. However, the k_1 values decrease from 2.99 × 10^{-3} µM^{-1} min^{-1} to 1.47 × 10^{-3} µM^{-1} min^{-1}, which may be attributed to high concentrations of penthiopyrad producing strong self-competition and thus reducing the reaction rates. These trends in kinetic parameters are similar to previously studied trends in the degradation of phenols, phenamine and antibiotics in the MnO$_2$ system,[24] which is consistent with the precursor complex kinetic model.[35]

3.2. DFT calculations and degradation pathways of penthiopyrad

In order to illustrate the possible degradation pathway of penthiopyrad by δ-MnO$_2$, the calculation of active sites vulnerable for an electrophilic reaction on penthiopyrad was performed using the condensed Fukui function. Based on the Hirshfeld charge distribution, the electrophilic sites (f^-) show plausible atoms in the penthiopyrad molecule for an electrophilic

reaction. As shown in Fig. 2, the iso-surface of f^- provides visualized Fukui function results after optimizing the calculation process. Moreover, the values of the condensed Fukui function are presented in Table 2, which can provide a quantitative version that a relatively large f^- value leads to a higher reaction probability. It is obvious that C18, C12 and S1 atoms hold relatively high f^- values, which suggest that these sites are more prone to electrophilic reactions, and may react with δ-MnO$_2$. Furthermore, the major degradation products of penthiopyrad are analyzed by HPLC-Q-TOF-MS and named P1–P7 (Fig. S7–S13†). Finally, the degradation pathway of penthiopyrad is proposed based on the reaction active sites and degradation products (Fig. 3).

Firstly, based on the Hirshfeld charge distribution, the C18 atom of the unsaturated double bond has the highest f^- (0.1346), and the C12 atom has the second highest f^- (0.1327), indicating that the olefin double bond in penthiopyrad is
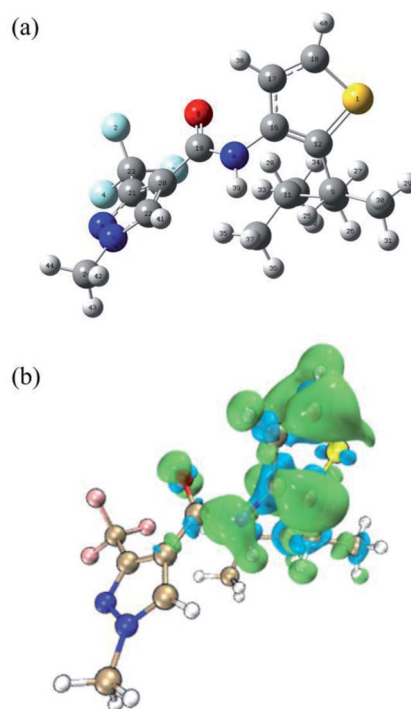
Fig. 2 The optimized geometry (a) isosurface; (b) f^- for the penthiopyrad molecule.

Table 2 Hirshfeld charge, and condensed Fukui functions (f^+), (f^-), (f^0) of penthiopyrad

Atom	Site	Number of electrons			Fukui functions		
		$N-1$	$N+1$	N	f^-	f^+	f^0
S	1	0.1827	0.0191	0.0612	0.1215	0.0421	0.0818
F	2	−0.1228	−0.1407	−0.1251	0.0022	0.0156	0.0089
F	3	−0.1056	−0.1209	−0.1076	0.0020	0.0134	0.0077
F	4	−0.1156	−0.1311	−0.1178	0.0021	0.0133	0.0077
O	5	−0.3167	−0.5128	−0.3635	0.0468	0.1492	0.0980
N	6	−0.0255	−0.1254	−0.0723	0.0468	0.0532	0.0500
N	7	0.0653	0.0244	0.0601	0.0052	0.0357	0.0204
N	8	−0.1468	−0.1985	−0.1554	0.0086	0.0430	0.0258
C	9	0.0034	−0.0161	−0.0124	0.0158	0.0038	0.0098
C	10	−0.0325	−0.0510	−0.0479	0.0154	0.0031	0.0093
C	11	−0.0181	−0.0216	−0.0207	0.0026	0.0009	0.0018
C	12	0.1043	−0.0564	−0.0284	0.1327	0.0280	0.0804
C	13	−0.0743	−0.0912	−0.0877	0.0134	0.0034	0.0084
C	14	−0.0853	−0.0922	−0.0899	0.0047	0.0022	0.0035
C	15	−0.0934	−0.0981	−0.0957	0.0023	0.0024	0.0024
C	16	0.1118	−0.0070	0.0051	0.1067	0.0122	0.0594
C	17	−0.0210	−0.0916	−0.0801	0.0591	0.0115	0.0353
C	18	0.0591	−0.0897	−0.0755	0.1346	0.0143	0.0744
C	19	0.1924	0.0283	0.1712	0.0212	0.1430	0.0821
C	20	−0.0582	−0.1175	−0.0615	0.0033	0.0560	0.0296
C	21	−0.0016	−0.0596	−0.0083	0.0067	0.0513	0.0290
C	22	0.0335	−0.0775	0.0240	0.0096	0.1014	0.0555
C	23	0.2948	0.2780	0.2932	0.0016	0.0152	0.0084
C	24	−0.0034	−0.0190	−0.0056	0.0021	0.0134	0.0078

electrophilic. The C atom of the olefin attacks the O atom in δ-MnO₂, and forms an intermediate epoxide (see pathway I and pathway II in Fig. 3). It is obvious that the δ-MnO₂ (Mn(IV/III)) is likely reduced to Mn(II) ions. The intermediate epoxide is unstable and is easily hydrolyzed to diketone products P1 ($m/z =$ 390, 7.317 min) and P2 ($m/z =$ 388, 9.298 min) under the acidic conditions (Fig. S7 and S8†). This electrophilic addition reaction is similar to the oxidation of carbamazepine.[33]

Secondly, it is easy for the S1 atom with the third-highest f^- (0.1215) value to attack the manganese atom in δ-MnO₂,[25,40] and form an intermediate complex as shown in pathway III in Fig. 3. With the electron transfer from the sulfur atom to the manganese atom, the penthiopyrad is degraded to form a sulfoxide (P3: $m/z =$ 376, 8.204 min) or a sulfone (P4: $m/z =$ 392, 6.739 min). The molecular structures of P3 and P4 are obtained from the MS spectra of P3 and P4 (Fig. S9 and S10†). As shown in Fig. 3, the molecular weights of P3 and P4 are 16 Da and 32 Da higher than that of the parent penthiopyrad, respectively, which suggests the formation of this intermediate by inserting one and two O atoms into the penthiopyrad molecule. As the oxidation reaction progresses, P3 can further degrade and transform into P5 ($m/z =$ 199, 6.152 min) as shown in Fig. S11.†

In addition, P6 ($m/z =$ 194, 4.026 min, in Fig. S12†) can be formed by direct hydrolysis of penthiopyrad, as shown in pathway IV in Fig. 3. Then the amino group of P6 is oxidized into a hydroxyl group, forming P7 ($m/z =$ 193, 4.047 min) as shown in Fig. S13.† These two compounds (P6 and P7) had also been identified as the metabolites of penthiopyrad degradation in soil under dark laboratory conditions and in field dissipation studies.[18]

3.3. Effect of environmental factors

To understand the degradation behavior of penthiopyrad in complex natural environments, the effects of some
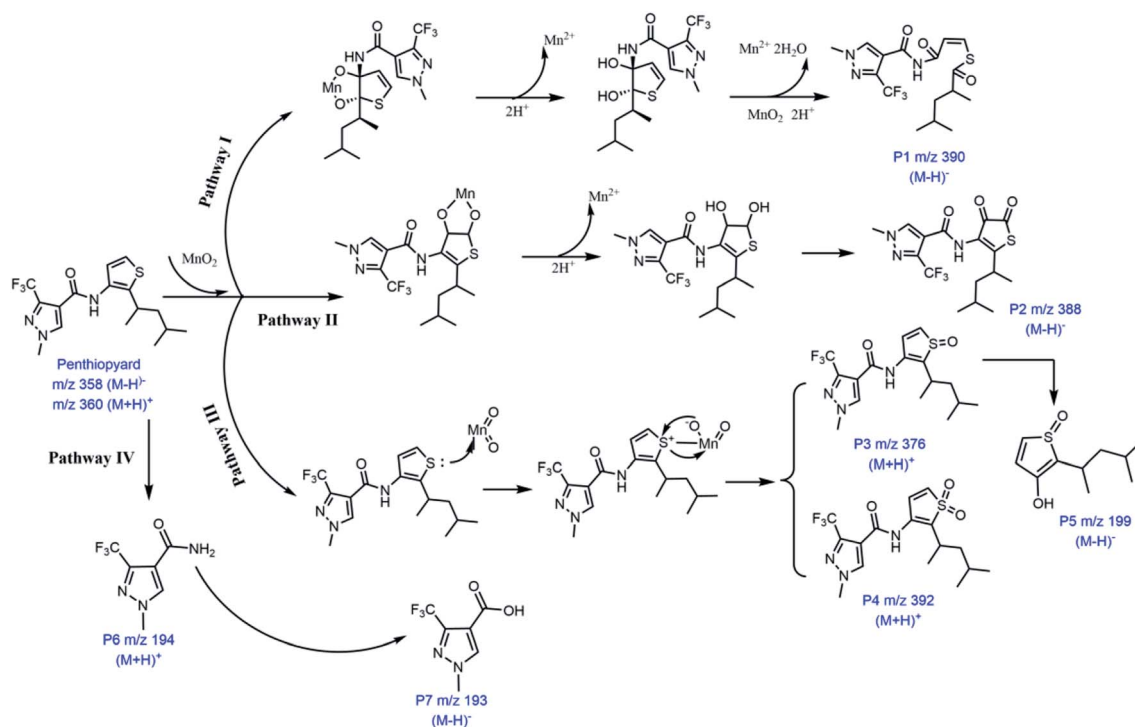
Fig. 3 Proposed degradation pathways of penthiopyrad.

environmental factors including pH, temperature, coexisting metal ions, and organic matter on the degradation of penthiopyrad by δ-MnO$_2$ were investigated.

3.3.1 Effects of solution pH. The degradation curves of penthiopyrad under different pH conditions are presented in Fig. S14.† It is observed that the degradation efficiency of penthiopyrad is 23.0% when the pH is 5.0, which increases to 37.3%, 75.8% and 92.5% when the pH values decrease to 4.4, 4.0 and 3.7. It indicates that the degradation efficiency of penthiopyrad increased with decreasing pH values. The degradation of penthiopyrad in the δ-MnO$_2$ system at different pH values is further described by eqn (1). As shown in Table 3, the apparent reaction rate constant (k_1) rapidly decreases from 6.71 × 10^{-3} μM^{-1} min^{-1} to 1.04 × 10^{-3} μM^{-1} min^{-1}, when pH increases from 3.70 to 5.00. This result indicates that a low pH value is beneficial to the degradation of penthiopyrad in the δ-MnO$_2$ system.

On the one hand, the pH value of the reaction solution affects the surface charge properties of δ-MnO$_2$. As shown in Fig. S15a,† the surface of δ-MnO$_2$ is negatively charged, and the amount of negative charge on the δ-MnO$_2$ surface will increase with the increasing pH value. Therefore, Mn^{2+} from the reduction product of MnO$_2$ can be adsorbed on the δ-MnO$_2$ surface by electrostatic interactions. Under high pH conditions, more Mn^{2+} will be adsorbed on the MnO$_2$ surface and occupy the reactive sites, thus inhibiting the degradation of penthiopyrad. On the other hand, the oxidation potential value (Φ (MnO$_2$/ Mn^{2+})) decreases from 0.79 V to 0.64 V when pH increases from 3.7 to 5.0 based on the Nernst equation (Fig. S15b†), which indicates that the increase of the solution pH value can decrease the oxidation capacity of δ-MnO$_2$. Therefore, an acidic environment is favorable for the degradation of penthiopyrad in the δ-MnO$_2$ system.

3.3.2 Effects of temperature. The influence of temperature on penthiopyrad degradation by δ-MnO$_2$ is given in Fig. S16a.† The degradation efficiency of penthiopyrad is 38.3% at 20 °C after 480 min, which is increased to 69.8% and 98.2% when the solution temperature increases to 30 °C and 40 °C, respectively. Furthermore, the degradation kinetics of penthiopyrad at different temperatures are estimated using eqn (1). As shown in Table 3, the apparent rate constants increase from 0.10 × 10^{-3} μM^{-1} min^{-1} to 3.07 × 10^{-3} μM^{-1} min^{-1} with the reaction temperature increase from 20 °C to 40 °C, which indicates that the reaction temperature has a significant effect on the degradation of penthiopyrad. Based on the Arrhenius equation, the value of the activation energy of penthiopyrad is calculated to be 43.21 kJ mol^{-1} (Fig. S16b†), which also supports that a warm environment is beneficial to the degradation of penthiopyrad in the δ-MnO$_2$ system.

3.3.3 Effects of metal cations. Some studies had reported that metal cations can affect the degradation of organic contaminants with δ-MnO$_2$.[24,38] In this study, the effects of metal cations including Mn^{2+}, Ca^{2+} and Mg^{2+} on the degradation of penthiopyrad by δ-MnO$_2$ are investigated. As shown in Fig. S17,† the degradation efficiencies of penthiopyrad are 9.3%, 35.3%, 41.5%, and 75.8% for Mn^{2+}, Ca^{2+}, Mg^{2+}, and the blank control, respectively. It is obvious that these metal cations exhibit obvious inhibition of penthiopyrad degradation, and the inhibition follows the order Mn^{2+} ≫ Ca^{2+} > Mg^{2+}. This result is consistent with the results in a previous study.[24] This inhibition by the metal cations is mainly attributed to the electrostatic interactions between the metal ions and δ-MnO$_2$. The negative charge surface of δ-MnO$_2$ can adsorb metal cations by electrostatic interactions, leading to metal ions occupying the active sites of manganese dioxide and interfering with the formation of precursor complexes between the penthiopyrad and manganese oxide. As shown in Table 3, the surface active sites S_1 decrease from 3.56 μM to 0.57 μM, 1.54 μM, and 1.84 μM, respectively, when Mn^{2+}, Ca^{2+} and Mg^{2+} are present in the reaction system. Compared to Ca^{2+} and Mg^{2+}, Mn^{2+} exhibits the strongest inhibitory effect on the penthiopyrad degradation. On the one hand, Mn^{2+} ion is the reduction product of MnO$_2$, and the newly added Mn^{2+} ion will lead to a higher concentration of Mn^{2+} in the reaction system and thus inhibit the penthiopyrad degradation by δ-MnO$_2$. On the other hand, the presence of Mn^{2+} also leads to the oxidation ability degradation of MnO$_2$ based on the Nernst equation. Therefore, Mn^{2+} ions exhibit the strongest inhibition compared to Ca^{2+} and Mg^{2+} ions.

Table 3 Effect of pH, temperature, inorganic ions and HA on k and S were obtained from fitting of experimental dates by eqn (1)

T (°C)	pH	δ-MnO$_2$ (mg L^{-1})	Penthiopyrad (μM)	Addition of ion or HA	S_1 (μM)	$k_1 \times 10^{-3}$ (μM^{-1} min^{-1})	R^2
30	4.00	150	4.00	Control	3.56	1.59 ± 0.03	0.998
30	3.70	150	4.00	—	3.81	6.71 ± 0.32	0.992
30	4.00	150	4.00	—	3.56	1.59 ± 0.03	0.998
30	4.40	150	4.00	—	1.42	1.26 ± 0.14	0.950
30	5.00	150	4.00	—	1.07	1.04 ± 0.08	0.955
20	4.00	150	4.00	—	1.90	0.10 ± 0.06	0.974
30	4.00	150	4.00	—	3.56	1.59 ± 0.03	0.998
40	4.00	150	4.00	—	3.98	3.07 ± 0.43	0.955
30	4.00	150	4.00	Mn^{2+} (0.1 mmol L^{-1})	0.56	0.51 ± 0.15	0.718
30	4.00	150	4.00	Ca^{2+} (0.1 mmol L^{-1})	1.54	1.32 ± 0.09	0.975
30	4.00	150	4.00	Mg^{2+} (0.1 mmol L^{-1})	1.84	1.38 ± 0.11	0.968
30	4.00	150	4.00	HA (5 mg L^{-1})	3.7	2.10 ± 0.11	0.978
30	4.00	150	4.00	HA (20 mg L^{-1})	3.9	2.50 ± 0.20	0.989

Considering Ca^{2+} and Mg^{2+}, Ca^{2+} has a slightly stronger inhibition effect on the penthiopyrad degradation than Mg^{2+}. This result may be attributed to the differences of the radii of Ca^{2+} and Mg^{2+}. The Ca^{2+} radius (99 pm) is larger than the Mg^{2+} radius (67 pm); thus calcium ions occupy a relatively large surface on MnO_2 and decrease the reaction surface area. Therefore, Ca^{2+} exhibits a slightly stronger inhibition effect on the degradation of penthiopyrad than Mg^{2+}.

3.3.4 Effects of HA. HA, as a natural organic compound, is commonly distributed in aquatic environments and has a potential impact on the degradation of many organic pollutants in natural systems.[41–43] In this study, the influence of HA on the degradation of penthiopyrad is presented Fig. S18a.† The co-existing HA obviously promotes the penthiopyrad degradation. As shown in Table 3, the k values increase from 1.59×10^{-3} μM^{-1} min^{-1} to 2.50×10^{-3} μM^{-1} min^{-1} with the increase of HA from 0 to 20 mg L^{-1}. This result indicates that HA is beneficial to the degradation of penthiopyrad in the δ-MnO_2 system, which is consistent with the degradation of bisphenol A and m-aminophenol in the MnO_2 system.[38,41] The degradation of organic contaminants by MnO_2 is accompanied by transformation from Mn(ɪᴠ) to Mn(ɪɪ), which is a self-inhibition process for MnO_2.[44] The FT-IR spectrum of the HA indicates that HA contains multiplefunctional groups such as carboxyl groups and phenolic hydroxyl groups (Fig. S18b†), which can combine with Mn^{2+} generated in the reaction.[45–47] This reaction will decrease the adsorption of Mn^{2+} ions on the surface of MnO_2 and weaken its self-inhibition process, thus increasing the oxidation ability of MnO_2. In addition, when HA is present in the solution, the active sites (i.e., S_1) increase slightly as shown in Table 3, which may be due to some Mn^{2+} ions being combined with HA molecules and also suggests that HA is beneficial to the degradation of penthiopyrad in the δ-MnO_2 system.

4. Conclusions

This study shows that penthiopyrad can be degraded efficiently by manganese dioxide, and the degradation kinetics of penthiopyrad is fitted by a complex model. The C18, C12, and S1 atoms of the penthiopyrad molecules are relatively highly reactive sites based on DFT calculations. The oxidation of thioether can form the degradation products of sulfoxide and sulfone, and the oxidation of olefin can form the degradation product of diketone. In addition, the hydrolysis products of penthiopyrad are also found. A reasonable degradation pathway of penthiopyrad in the δ-MnO_2 system is proposed. The environmental conditions obviously affect the degradation of penthiopyrad in the δ-MnO_2 system. A high temperature and low pH are beneficial to the degradation of penthiopyrad in the δ-MnO_2 system. Co-existing metal ions (Mn^{2+}, Ca^{2+}, and Mg^{2+}) compete for the active sites with penthiopyrad, leading to inhibition of the degradation of penthiopyrad. Co-existing HA can promote the penthiopyrad degradation by combining with Mn^{2+} generated in the reaction, and weakening its self-inhibition process. It has been reported that sulfoxide-type products have high genotoxicity. Therefore, the potential ecological risk of penthiopyrad degradation products in natural environments should be assessed, because one of the degradation products of penthiopyrad is a sulfoxide.

Conflicts of interest

The authors declared that they have no conflicts of interest to this work.

Acknowledgements

References

1 T. Joseph-Horne and D. W. Hollomon, Molecular mechanisms of azole resistance in Fungi, *FEMS Microbiol. Lett.*, 1997, **149**, 141–149.

2 X. Mao, Y. Wang, Y. Hou and M. Zhou, Activity of the Succinate Dehydrogenase Inhibitor Fungicide Penthiopyrad Against Sclerotinia sclerotiorum, *Plant Dis.*, 2020, **104**(10), 2696–2703.

3 S. Wu, L. Lei, M. Liu, Y. Song, S. Lu, D. Li, H. Shi, K. M. Raley-Susman and D. He, Single and mixture toxicity of strobilurin and SDHI fungicides to Xenopus tropicalis embryos, *Ecotoxicol. Environ. Saf.*, 2018, **153**, 8–15.

4 D. Steinhauer, M. Salat, R. Frey, A. Mosbach, T. Luksch, D. Balmer, R. Hansen, S. Widdison, G. Logan, R. A. Dietrich, G. H. J. Kema, S. Bieri, H. Sierotzki, S. F. F. Torriani and G. Scalliet, A dispensable paralog of succinate dehydrogenase subunit C mediates standing resistance towards a subclass of SDHI fungicides in Zymoseptoria tritici, *PLoS Pathog.*, 2019, **15**(12), e1007780.

5 N. C. Anasco, J. Koyama and S. Uno, Pesticide residues in coastal waters affected by rice paddy effluents temporarily stored in a wastewater reservoir in southern Japan, *Arch. Environ. Contam. Toxicol.*, 2010, **58**(2), 352–360.

6 A. Abad-Fuentes, E. Ceballos-Alcantarilla, J. V. Mercader, C. Agullo, A. Abad-Somovilla and F. A. Esteve-Turrillas, Determination of succinate-dehydrogenase-inhibitor fungicide residues in fruits and vegetables by liquid chromatography-tandem mass spectrometry, *Anal. Bioanal. Chem.*, 2015, **407**(14), 4207–4211.

7 H. T. Vu, M. J. Keough, S. M. Long and V. J. Pettigrove, Effects of the boscalid fungicide Filan(R) on the marine amphipod Allorchestes compressa at environmentally relevant concentrations, *Environ. Toxicol. Chem.*, 2016, **35**(5), 1130–1137.

8 C. M. Stephens, J. P. Kerns, K. A. Ahmed and T. W. Gannon, Influence of post-application irrigation and mowing timing on fungicide fate on a United States Golf Association golf course putting green, *J. Environ. Qual.*, 2021, **50**(4), 868–876.

9 F. Tian, C. Qiao, J. Luo, L. Guo, T. Pang, R. Pang, J. Li, C. Wang, R. Wang and H. Xi, Development of a fast multi-

residue method for the determination of succinate dehydrogenase inhibitor fungicides in cereals,vegetables and fruits by modified QuEChERS and UHPLC-MS/MS, *J. Chromatogr. B: Anal. Technol. Biomed. Life Sci.*, 2020, **1152**, 1222612.

10 A. Brenet, R. Hassan-Abdi and N. Soussi-Yanicostas, Bixafen, a succinate dehydrogenase inhibitor fungicide, causes microcephaly and motor neuron axon defects during development, *Chemosphere*, 2021, **265**, 128781.

11 F. He, J. Wan, X. Li, S. Chu, N. Sun and R. Liu, Toxic effects of benzovindiflupyr, a new SDHI-type fungicide on earthworms (Eisenia fetida), *Environ. Sci. Pollut. Res.*, 2021, 1–14.

12 P. Benit, A. Kahn, D. Chretien, S. Bortoli, L. Huc, M. Schiff, A. P. Gimenez-Roqueplo, J. Favier, P. Gressens, M. Rak and P. Rustin, Evolutionarily conserved susceptibility of the mitochondrial respiratory chain to SDHI pesticides and its consequence on the impact of SDHIs on human cultured cells, *PLoS One*, 2019, **14**(11), e0224132.

13 Y. Yanase, H. Katsuta, K. Tomiya, M. Enomoto and O. Sakamoto, Development of a novel fungicide, penthiopyrad, *J. Pestic. Sci.*, 2013, **38**(3), 167–168.

14 H. H. Noh, J. Y. Lee, H. K. Park, J. W. Lee, S. H. Jo, J. B. Lim, H. G. Shin, H. Kwon and K. S. Kyung, Dissipation, persistence, and risk assessment of fluxapyroxad and penthiopyrad residues in perilla leaf (Perilla frutescens var. japonica Hara), *PLoS One*, 2019, **14**(4), e0212209.

15 EFSA (European Food Safety Authority), Reasoned opinion on the setting of new MRLs for penthiopyrad in various crops, *EFSA J.*, 2012, **10**(10), 2948.

16 M. Podbielska, M. Kus-Liskiewicz, B. Jagusztyn, B. Piechowicz, S. Sadlo, M. Slowik-Borowiec, M. Twaruzek and E. Szpyrka, Influence of Bacillus subtilis and Trichoderma harzianum on Penthiopyrad Degradation under Laboratory and Field Studies, *Molecules*, 2020, **25**(6), 1241.

17 E. Ceballos-Alcantarilla, A. Abad-Fuentes, C. Agulló, A. Abad-Somovilla and J. V. Mercader, Immunochemical method for penthiopyrad detection through thermodynamic and kinetic characterization of monoclonal antibodies, *Talanta*, 2021, **226**, 122123.

18 EFSA (European Food Safety Authority), Conclusion on the peer review of the pesticide risk assessment of the active substance penthiopyrad, *EFSA J.*, 2013, **11**(2), 3111.

19 L. Qian, S. Qi, F. Cao, J. Zhang, C. Li, M. Song and C. Wang, Effects of penthiopyrad on the development and behaviour of zebrafish in early-life stages, *Chemosphere*, 2019, **214**, 184–194.

20 W. Liu, N. B. Sutton, H. H. M. Rijnaarts and A. A. M. Langenhoff, Anoxic conditions are beneficial for abiotic diclofenac removal from water with manganese oxide (MnO_2), *Environ. Sci. Pollut. Res.*, 2018, **25**, 10141–10147.

21 S. C. Hafner and S. J. Parikh, Sorption and abiotic transformation of monensin by iron and manganese oxides, *Chemosphere*, 2020, **253**, 126623.

22 W. Zhao, H. Cheng and S. Tao, Structure-Reactivity Relationships in the Adsorption and Degradation of Substituted Phenylarsonic Acids on Birnessite (delta-MnO_2), *Environ. Sci. Technol.*, 2020, **54**(3), 1475–1483.

23 B. Sun, Y. Zhang, Z. Gong, J. Zhang and J. Zhang, Reducing substances-enhanced degradation of pollutants by permanganate: the role of in situ formed colloidal MnO_2, *Chemosphere*, 2021, **276**, 130203.

24 S. Y. Liou and W. R. Chen, Oxidative transformation kinetics and pathways of albendazole from reactions with manganese dioxide, *J. Hazard. Mater.*, 2018, **347**, 299–306.

25 M. H. Hsu, T. H. Kuo, Y. E. Chen, C. H. Huang, C. C. Hsu and A. Y. Lin, Substructure Reactivity Affecting the Manganese Dioxide Oxidation of Cephalosporins, *Environ. Sci. Technol.*, 2018, **52**(16), 9188–9195.

26 J. Cheng, D. D. Wang, B. H. Wang, H. Ning, Y. Zhang, Y. C. Li, J. T. An and P. L. Gao, Plasma-catalytic degradation of ciprofloxacin in aqueous solution over different MnO_2 nanocrystals in a dielectric barrier discharge system, *Chemosphere*, 2020, **253**, 126595.

27 F. Hashemzadeh, M. Mehdi Kashani Motlagh and A. Maghsoudipour, A comparative study of hydrothermal and sol–gel methods in the synthesis of MnO_2 nanostructures, *J. Sol-Gel Sci. Technol.*, 2009, **51**(2), 169–174.

28 M. J. Frisch, G. W. Trucks, H. B. Schlegel, G. E. Scuseria, M. A. Robb, J. R. Cheeseman, G. Scalmani, V. Barone, B. Mennucci, G. A. Petersson, H. Nakatsuji, M. Caricato, X. Li, H. P. Hratchian, A. F. Izmaylov, J. Bloino, G. Zheng, J. L. Sonnenberg, M. Hada, M. Ehara, K. Toyota, R. Fukuda, J. Hasegawa, M. Ishida, T. Nakajima, Y. Honda, O. Kitao, H. Nakai, T. Vreven, J. A. Montgomery Jr, J. E. Peralta, F. Ogliaro, M. Bearpark, J. J. Heyd, E. Brothers, K. N. Kudin, V. N. Staroverov, R. Kobayashi, J. Normand, K. Raghavachari, A. Rendell, J. C. Burant, S. S. Iyengar, J. Tomasi, M. Cossi, N. Rega, J. M. Millam, M. Klene, J. E. Knox, J. B. Cross, V. Bakken, C. Adamo, J. Jaramillo, R. Gomperts, R. E. Stratmann, O. Yazyev, A. J. Austin, R. Cammi, C. Pomelli, J. W. Ochterski, R. L. Martin, K. Morokuma, V. G. Zakrzewski, G. A. Voth, P. Salvador, J. J. Dannenberg, S. Dapprich, A. D. Daniels, Ö. Farkas, J. B. Foresman, J. V. Ortiz, J. Cioslowski and D. J. Fox, *Gaussian 09*, Gaussian, Inc., Wallingford, CT, USA, 2009.

29 T. Lu and F. Chen, Multiwfn: a multifunctional wavefunction analyzer, *J. Comput. Chem.*, 2012, **33**, 580–592.

30 J. Peng, H. Zhou, W. Liu, Z. Ao, H. Ji, Y. Liu, S. Su, G. Yao and B. Lai, Insights into heterogeneous catalytic activation of peroxymonosulfate by natural chalcopyrite: pH-dependent radical generation, degradation pathway and mechanism, *Chem. Eng. J.*, 2020, **397**, 125387.

31 W. Kong, Y. Gao, Q. Yue, Q. Li, B. Gao, Y. Kong, X. Wang, P. Zhang and Y. Wang, Performance optimization of CdS precipitated graphene oxide/polyacrylic acid composite for efficient photodegradation of chlortetracycline, *J. Hazard. Mater.*, 2020, **388**, 121780.

32 W. Liu, Y. Li, F. Liu, W. Jiang, D. Zhang and J. Liang, Visible-light-driven photocatalytic degradation of diclofenac by carbon quantum dots modified porous g-C_3N_4:

mechanisms, degradation pathway and DFT calculation, *Water Res.*, 2019, **151**, 8–19.

33 J. Zhai, Q. Wang, Q. Li, B. Shang, M. H. Rahaman, J. Liang, J. Ji and W. Liu, Degradation mechanisms of carbamazepine by delta-MnO$_2$: role of protonation of degradation intermediates, *Sci. Total Environ.*, 2018, **640–641**, 981–988.

34 W. R. Chen and C. H. Huang, Transformation kinetics and pathways of tetracycline antibiotics with manganese oxide, *Environ. Pollut.*, 2011, **159**(5), 1092–1100.

35 H. Zhang, W. R. Chen and C. H. Huang, Kinetic modeling of oxidation of antibacterial agents by manganese oxide, *Environ. Sci. Technol.*, 2008, **42**(15), 5548–5554.

36 L. Carena, M. Minella, F. Barsotti, M. Brigante, M. Milan, A. Ferrero, S. Berto, C. Minero and D. Vione, Phototransformation of the Herbicide Propanil in Paddy Field Water, *Environ. Sci. Technol.*, 2017, **51**(5), 2695–2704.

37 D. la Cecilia and F. Maggi, Analysis of glyphosate degradation in a soil microcosm, *Environ. Pollut.*, 2018, **233**, 201–207.

38 W. Huang, G. Wu, H. Xiao, H. Song, S. Gan, S. Ruan, Z. Gao and J. Song, Transformation of m-aminophenol by birnessite (delta-MnO$_2$) mediated oxidative processes: reaction kinetics, pathways and toxicity assessment, *Environ. Pollut.*, 2020, **256**, 113408.

39 H. Xiao, H. Song, H. Xie, W. Huang, J. Tan and J. Wu, Transformation of acetaminophen using manganese dioxide-mediated oxidative processes: reaction rates and pathways, *J. Hazard. Mater.*, 2013, **250–251**, 138–146.

40 L. Li, D. Wei, G. Wei and Y. Du, Product identification and the mechanisms involved in the transformation of cefazolin by birnessite (δ-MnO$_2$), *Chem. Eng. J.*, 2017, **320**, 116–123.

41 K. Lin, Y. Peng, X. Huang and J. Ding, Transformation of bisphenol A by manganese oxide-coated sand, *Environ. Sci. Pollut. Res.*, 2013, **20**, 1461–1467.

42 K. Xu, W. Ben, W. Ling, Y. Zhang, J. Qu and Z. Qiang, Impact of humic acid on the degradation of levofloxacin by aqueous permanganate: kinetics and mechanism, *Water Res.*, 2017, **123**, 67–74.

43 J. F. Yang, M. He, T. F. Wu, A. P. Hao, S. B. Zhang, Y. D. Chen, S. B. Zhou, L. Y. Zhen, R. Wang, Z. L. Yuan and L. Deng, Sulfadiazine oxidation by permanganate: kinetics, mechanistic investigation and toxicity evaluation, *Chem. Eng. J.*, 2018, **349**, 56–65.

44 K. Lin, W. Liu and J. Gan, Reaction of Tetrabromobisphenol A (TBBPA) with Manganese Dioxide: Kinetics, Products, and Pathways, *Environ. Sci. Technol.*, 2009, **43**, 4480–4486.

45 I. Christl, C. J. Milne, D. G. Kinniburgh and R. Kretzschmar, Relating ion binding by fulvic and humic acids to chemical composition and molecular size. 2. Metal binding, *Environ. Sci. Technol.*, 2001, **35**, 2512–2517.

46 K. H. Kang, J. Dec, H. Park and J. M. Bollag, Effect of phenolic mediators and humic acid on cyprodinil transformation in presence of birnessite, *Water Res.*, 2004, **38**, 2737–2745.

47 A. G. Liu and R. D. Gonzalez, Modeling adsorption of copper(II), cadmium(II) and lead(II) on purified humic acid, *Langmuir*, 2000, **16**, 3902–3909.